Modeling Wind Turbines to Assess Impact of Offshore Wind Farms on Maritime X- and S-band Radars

Krzysztof Bronk, Patryk Koncicki, Adam Lipka, Rafał Niski, and Błażej Wereszko

National Institute of Telecommunications, Warsaw, Poland

https://doi.org/10.26636/jtit.2024.1.1484

Abstract — This article discusses several aspects related to modeling the impact of offshore wind farms on maritime radar systems operating in the X and S bands. The first part of the paper focuses on theoretical models and analyses, taking into account radio shadowing and false radar echoes. Additionally, the issue of spatial modeling of wind turbines, with diffraction phenomena considered, is reviewed with the help of suitable propagation models. By relaying on a software-based implementation of the proposed model, the authors carried out a detailed simulation of the impact of wind turbines on radar systems operating in the X and S bands. The results of these simulations are presented and discussed in the second part of the article.

Keywords — false radar echoes, offshore wind farm, radar systems, radiolocation, radio shadowing, radio wave propagation

1. Introduction

Renewable energy sources become increasingly popular around the world. Their growth outpaces that of conventional energy sources, and wind energy is one of areas characterized by the highest growth rate. Statistics from the latest GWEC Global Wind Report 2023 [1] show that 77.6 GW of new wind power capacity was connected to power grids in 2022 globally, bringing the total installed wind capacity to 906 GW (a growth rate of 9% compared with 2021). Global installed wind energy capacity reached 1 terawatt (TW) in June 2023, and the expectations are it will reach 2 TW over the next 7 years.

Development of the wind energy sector relies, globally, on two primary segments: onshore wind power and offshore wind power, with the latter now becoming an area that is characterized by an enormous development potential. Turbines are built further away from the coast and their physical dimensions are growing as well – see Fig. 1. This applies both to individual turbines which are based on higher masts, have larger blades and larger generators capable of producing more power, and to complete wind farms comprising dozens or even hundreds of units.

On the other hand, offshore wind farms (OWF) rely on larger and more densely clustered structures which worsen the propagation conditions prevailing in such an environment. This creates the need to analyze and evaluate the impact of the emerging offshore turbines on critical radiocommunication systems. In the case of offshore wind farms, their impact on radiolocation systems is a very important element of this evaluation. Systems which are potentially affected are used by maritime administrations, the navy, the border guard, the coast guard, etc.

In Poland, every investor intending to erect and operate an offshore wind farm in the Polish exclusive economic zone (EEZ) is obligated by law to submit an expert opinion discussing the potential impact of the planned farm on critical maritime systems. If any negative impact is anticipated, appropriate mitigation measures must be proposed and implemented. Such expert opinions must be submitted before any construction work commences and a failure to do so results in the investor's application being rejected. Such requirements are in effect in the specific Polish legal landscape, but they clearly underline the significance of this issue.

Since 2013, the authors have been drawing up expert opinions focusing on the impact that OWFs exert on radio communication and radar systems, and the National Institute of Telecommunications is the only entity in Poland that is actively involved in the preparation of such expert opinions for investors intending to build OWFs in the Polish EEZ.

It should be noted that no coherent and comprehensive methodology exists for assessing the impact of OWFs on radar systems that would take into account their specific nature and key physical phenomena. No official standard exists which would serve as a background for such an analysis. In 2011, ITU-R issued the first version of the BT.1893 recommendation [2] which provides the mathematical background for the assessment of impairments caused by land wind farms. The said recommendation was originally dedicated to digital television systems operating in the UHF band (300–3000 MHz). The applicability of this recommendation was expanded in the following years by the authors [3], [4]. On the other hand, a radar-based theory regarding the so-called radar cross section (RCS) of a wind turbine has been known for many years now. In both the ITU-R recommendation and the RCS theory, the manner in which signals are reflected by the turbines (their blades, mast, etc.) is the key phenomenon taken into consideration. Offshore wind farms are generally much bigger structures than their land-based counterparts. This applies to all of their components: masts, blades, etc. To put

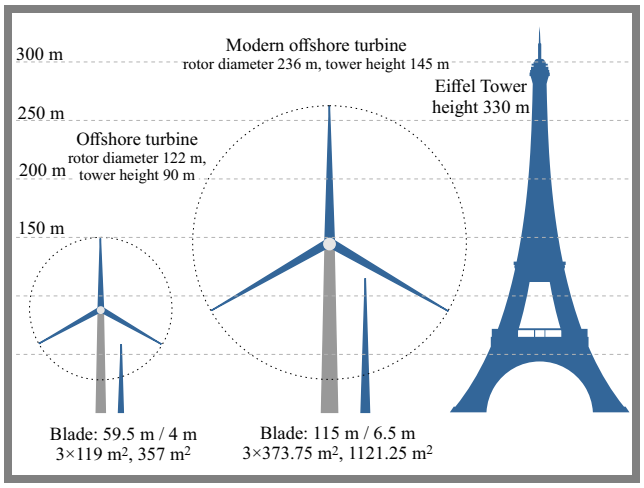

Fig. 1. Comparison of the sizes of wind turbines erected in recent years (the Eiffel Tower is shown in the drawing for scale).

in the simplest terms: offshore farms have a much greater reflecting surface.

All the theoretical aspects that need to be taken into consideration to analyze the impact of OWFs on radiolocation systems will be presented in Sections 2 and 3 of this paper. That includes the elements of the ITU-R BT.1893 recommendation which are particularly relevant to the subject of this paper.

In Section 4, the article describes the methodology applied to assess the impact of OWFs on radar systems in the context of the radio shadowing and false radar echoes. Finally, simulation-based analyses of coastal and ship radar systems operating in the X and S bands, performed using the newly created maritime wind turbine model, are presented and discussed in Section 5. Determination of the corrective measures that are required (if any) to minimize the unfavorable impact of turbines on radar systems is a very important aspect as well. Section 6 concludes the research and provides a future outlook.

2. Mathematical Foundations

2.1. ITU-R BT.1893-1 Model

Two methods were adopted for the purpose of investigating the impact of wind turbines on radio communication systems and properly modeling the radio channel, as described in recommendation ITU-R BT.1893-1 "Assessment methods of impairment caused to digital TV reception by wind turbines" [2]. The first of these methods – described in Annex 1 of the recommendation – models the propagation for a wind farm as a whole (i.e. without distinguishing between individual turbines). Annex 2 introduces a model describing the propagation of the radio signal in the presence of a wind farm, applicable to near field scenarios. This model considers each turbine as a separate obstacle. Consequently, this method will only be applicable to studies focusing on the farm's impact on ship terminals which may be located in close proximity to the turbines, while in other cases, the method described in Annex 1 should be used.

2.2. Effective Reflecting Surface

Effective reflecting surface is known as radar cross section (RCS), since this concept is derived from radar technology. RCS describes the ability of an object to reflect radio (radar) or sound waves. It is expressed as an area, in [m^2], situated on a plane that is perpendicular to the direction of the incident wave, which, in the case of ideal, isotropic, reflection of all the energy incident on it, would produce the same equivalent, isotropically radiated power as the power generated by the real object. Factors that affect the RCS value include the following [5]:

- size of the object's cross-sectional area,
- shape of the object,
- material the object is made of or covered with,
- frequency of the signal reflected from the object,
- angle of incidence of the signal,
- signal reflection angle,
- polarization of the transmitted and received signal in relation to the target,
- strength of the radar signal,
- distance between the radar and the target.

Objects with a larger effective reflection surface will reflect waves better, i.e. will generate a stronger echo. Therefore, they can be detected from a greater distance. In electromagnetic analysis, the formula for the RCS parameter, most often denoted by σ, can be presented as follows:

$$\sigma = \lim_{r\to\infty} 4\pi r^2 \frac{|E_s|^2}{|E_i|^2} , \tag{1}$$

where E_i is the intensity of the electric field incident on the object and E_s is the intensity of the electric field scattered on the object.

From the point of view of this article, the RCS parameter can be defined, in its analytical form, as [6]:

$$\sigma_{MAX} = \frac{4\pi\, 9D^2S^2}{\lambda^2} , \tag{2}$$

where S is average blade width [m], D is blade length [m] and λ is wavelength [m].

Assuming that:

$$3 \cdot D \cdot S = A , \tag{3}$$

where A [m^2] is the equivalent of the total blade area, we obtain a simplified version of Eq. (2):

$$\sigma_{MAX} = \frac{4\pi A^2}{\lambda^2} , \tag{4}$$

Depending on the distance between the transmitter and the wind turbine, an appropriate mathematical formula is used to calculate value of the RCS parameter. The application of such a formula depends on the fulfillment of the far-field criterion. If this criterion is met, formulas from Annex 1 are used to calculate RCS [7]–[9]. In this case, the reflection of the signal from the wind turbine's rotors is taken into account, where the calculation should primarily consider the equivalent area of the blades of the wind turbine. However, if the far-field criterion is not met, formulas from Annex 2 are

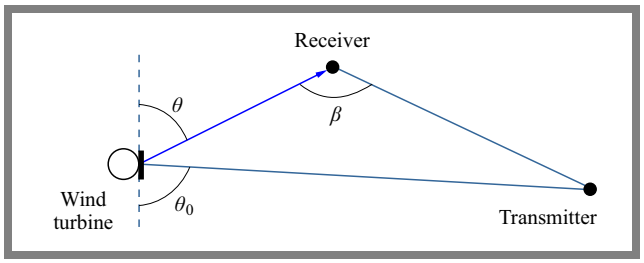

Fig. 2. Graphic interpretation of the angles from Eq. (6).

used for calculations, where mainly the reflection from the wind turbine mast, characterized by its radius, is taken into account.

In general, the effective reflecting surface for Annex 1 can be described by:

$$RCS_{A1}[\mathrm{dBm}^2] = 10\log\frac{4\pi A^2}{\lambda^2} + 10\log f_v(\theta) + 10\log f_h(\theta) + L_{mat}(\varepsilon_r)\ , \tag{5}$$

where:

lower index $_{A1}$ indicates the formula is true for Annex 1 of [2],
A – equivalent of the total area of the blades [m^2],
λ – wavelength [m],
S – mean width of the wind blade [m],
$f_h(\theta)$ – directional reflection function of the signal from the turbine in the horizontal plane,
$f_v(\theta)$ – directional reflection function of the signal from the turbine in the vertical plane,
$f(\theta) = g(\theta)^2$,

$$g(\theta) = \mathrm{sinc}^2\left[\frac{S}{\lambda}(\cos\theta - \cos\theta_0)\right]\sin\theta\ , \tag{6}$$

$$\mathrm{sinc}(x) = \frac{\sin(\pi x)}{\pi x}$$

$L_{mat}(\varepsilon_r)$ – losses related to the relative permeability of the turbine blade material.

The graphic interpretation of the angles referred to Eq. (6) is presented in Fig. 2 [2]. To compare the RCS parameters for both annexes, the losses resulting from the material and the antenna angles were temporarily omitted. Ultimately, the following formula was reached for Annex 1 [6]:

$$RCS_{A1,MAX}[\mathrm{dBm}^2] = \sigma_{A1,MAX}[\mathrm{dBm}^2] = 10\log\frac{4\pi A^2}{\lambda^2} + L_{mat}(\varepsilon_r)\ . \tag{7}$$

To discuss the impact the material the blades of the wind turbine are made of on the reflection of the signal, the L_{mat} coefficient has been introduced. For a broader analysis of this issue, the concept of wave reflection coefficient should be presented, i.e. the ratio of the intensity of the reflected wave to the intensity of the incident wave. An electromagnetic wave falling on the boundary surface of two media with given refractive indices is refracted and partially reflected. In general terms, the wave reflection coefficient can be described by [10]:

$$L_{mat}\ [\mathrm{dB}] = 20\log|\gamma|\ , \tag{8}$$

where:

$$\gamma = \frac{Z - Z_0}{Z + Z_0} \tag{9}$$

Z is the wave impedance of the electromagnetic wave, which in the case of an ideal dielectric, i.e. one where the conductivity is close to 0, can be described as:

$$Z = \sqrt{\frac{\mu}{\varepsilon}}\ , \tag{10}$$

where μ is the magnetic permeability and ε is the electrical permittivity.

Z_0 in Eq. (9) denotes the wave impedance in free space and is expressed by:

$$Z_0 = \sqrt{\frac{\mu_0}{\varepsilon_0}} \approx 120\,\pi\Omega \approx 376.7\ \Omega\ . \tag{11}$$

Using the above formulas, it is possible to determine the value of the reflection wave coefficient applicable to the case at hand. Modern wind turbine blades are usually made of fiberglass or fiberglass reinforced plastics (GFRP) [11]. In order to calculate the value of the reflection wave coefficient, it was determined that the relative permittivity of GFRP assumes the following values: $\varepsilon_r = 3.3 \div 4.2$ [12]. In an isotropic, homogeneous dielectric with negligible magnetic properties, i.e. $\mu = \mu_0 = 4\pi \times 10^{-7}$ [H/m] and $\varepsilon = \varepsilon_r \times 8.854 \times 10^{-12}$ [F/m], this means that the value of the wave impedance can be calculated from a simplified formula:

$$Z = \sqrt{\frac{\mu}{\varepsilon}} = \sqrt{\frac{\mu_0}{\varepsilon_0\varepsilon_r}} = \frac{Z_0}{\sqrt{\varepsilon_r}} = \frac{377}{\sqrt{\varepsilon_r}}\ \Omega\ , \tag{12}$$

where for GFRP we can assume $\mu = \mu_0$ [13] and the range of the reflection wave coefficient is:

$$L_{mat_{\varepsilon_r=3.3}}\ [\mathrm{dB}] = 20\log(|\gamma|) = 20\log\left|\frac{Z - Z_0}{Z + Z_0}\right| = 20\log\left|\frac{\frac{377}{\sqrt{3.3}} - Z_0}{\frac{377}{\sqrt{3.3}} + Z_0}\right| = -10.97\ ,$$

$$L_{mat_{\varepsilon_r=4.2}}\ [\mathrm{dB}] = 20\log(|\gamma|) = 20\log\left|\frac{Z - Z_0}{Z + Z_0}\right| = 20\log\left|\frac{\frac{377}{\sqrt{4.2}} - Z_0}{\frac{377}{\sqrt{4.2}} + Z_0}\right| = -9.25\ .$$

Modern turbine blades are often made of GFRP material with $\varepsilon_r = 4.2$, with its reflectance equaling approx. 9 dB. It was therefore assumed in the calculations that the theoretical reflection would be reduced by 9 dB.

Mismatch loss (ML) is another important concept that needs to be taken into consideration. This is a measure of how much the transmitted power is attenuated due to the reflection. For the purpose of presenting a simulation modeling the presence of offshore wind turbines in radar areas, the value of the ML coefficient for a turbine made of GFRP with $\varepsilon_r = 4.2$ was calculated as:

$$ML\ [\mathrm{dB}] = -10\log(1 - |\gamma|^2) = -10\log\left(1 - \left|\frac{Z - Z_0}{Z + Z_0}\right|^2\right) = -10\log\left(1 - \left|\frac{\frac{377}{\sqrt{4.2}} - Z_0}{\frac{377}{\sqrt{4.2}} + Z_0}\right|^2\right) \approx 0.6\ . \tag{13}$$

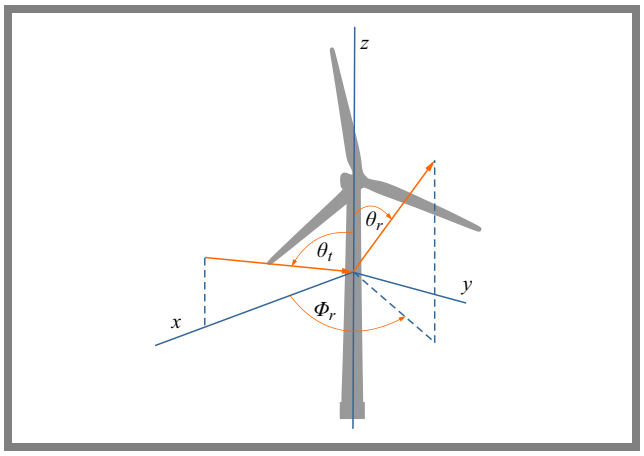

Fig. 3. Graphic interpretation of the angles from Eq. (14).

This means that radar signal strength will decrease by 0.6 dB after passing through the turbine area.

The parameter σ_{A2}, i.e. RCS of the turbine mast towards the receiving antenna for Annex 2 can be calculated from:

$$\sigma_{A2}(\phi_r, \theta_t) = krL_{nf}^2 \sqrt{\frac{1+\cos\phi_r}{2}} \sin\theta_t \ , \tag{14}$$

where:

lower index $_{A2}$ indicates the formula is true for Annex 2 of [2],

$k = \dfrac{2\pi}{\lambda}$ [1/m],

r – tower radius [m],

ϕ_r – receive antenna's angular position in the horizontal plane, measured at the wind turbine under consideration, anti-clockwise from the direction of the transmit antenna,

θ_t – transmit antenna's angular position in the vertical plane.

The graphic interpretation of the angles referred to in Eq. (14) is presented in Fig. 3. It should be noted that for distances at which the effect of the turbines may be significant, the far field criterion is usually not met, as in general:

$$R_{Tx-WT_i} < \frac{2L^2}{\lambda} \ , \tag{15}$$

where L is the height [m] of the transmitting antenna.

In this case, the near-field scattering effects should be taken into account when considering the near-field tower height L_{nf} [m]:

$$L_{nf} = \sqrt{\frac{\lambda R_{Tx-WT_i}}{2}} \ . \tag{16}$$

The inequality specified in Eq. (15) should be considered as the upper bound for applicability of Annex 2. If this inequality is no longer true (for higher values of R_{Tx-WTi}), Annex 1 should be applied instead.

The mean amplitude of each path can be determined as the ratio of the power of the reflected (unwanted) component to the direct (wanted) component:

$$P_i = 10\log\frac{P_{Tx-WT_i-Rx}}{P_{Tx-Rx}} \ . \tag{17}$$

Components for which the mean P_i amplitude is less than –45 dB should be ignored as insignificant. To compare the RCS formula for Annex 2 with the formula for Annex 1 from Eq. (7), we can convert Eq. (14) to:

$$RCS_{A2}[\mathrm{dBm}^2] = \sigma_{A2,MAX}[\mathrm{dBm}^2] + 10\log f_{A2}(\phi_r) \tag{18}$$

where:

$$f_{A2}(\phi_r) = \sqrt{\frac{1+\cos\phi_r}{2}} \sin\theta_t \ ,$$

$$RCS_{A2,MAX}[\mathrm{dBm}^2] = \sigma_{A2,MAX}[\mathrm{dBm}^2] = 10\log(krL_{nf}^2). \tag{19}$$

For Annex 1, the RCS takes a constant value, because it does not depend on distance. On the other hand, for Annex 2, by substituting the relation (16) to Eq. (19) one can notice a change in the RCS value [14] depending on the distance between the turbine and the transmitter.

The formulas defining the value of unwanted power, i.e. power reflected from the turbine, represented by the unwanted field strength (P_{UFSR}), also vary for the two Annexes. In the case of Annex 1, it can be defined as:

$$P_{UFSR_{Annex1}} = EIRP - L_t + 20\log\rho \ , \tag{20}$$

where:

$EIRP$ – equivalent isotropical radiated power of the transmitter [dBm],

L_t – propagation attenuation on the transmitter-turbine path [dB],

ρ – scattering coefficient:

$$\rho = \frac{A}{\lambda r} g(\theta) \ , \tag{21}$$

where r is the distance between the turbine and the receiver [m] and $g(\theta)$ is the function defined by Eq. (6).

For Annex 2, the P_{UFSR} can be described as:

$$P_{UFSR_{Tx-WT_i-Rx RCS2}} = \frac{P_t G_{Tx-WT_i} G_{Rx-WT_i} \lambda^2 \sigma_{A2,MAX}}{(4\pi)^3 R_{Tx-WT_i}^2 R_{WT_i-Rx}^2} = \frac{P_t G_{Tx-WT_i} G_{Rx-WT_i} \lambda^2 r}{4(4\pi)^2 R_{Tx-WT_i} R_{WT_i-Rx}^2} \ . \tag{22}$$

After transformation, the formula defining P_{UFSR} for Annex 1 can be expressed in a similar way as the Annex 2 P_{UFSR}:

$$P_{UFSR_{Tx-WT_i-Rx RCS1}} = \frac{P_t G_{Tx-WT_i} G_{Rx-WT_i} \lambda^2 \sigma_{A1,MAX}}{(4\pi)^3 R_{Tx-WT_i}^2 R_{WT_i-Rx}^2} = \frac{P_t G_{Tx-WT_i} G_{Rx-WT_i} A^2}{(4\pi)^2 R_{Tx-WT_i}^2 R_{WT_i-Rx}^2} \ . \tag{23}$$

3. Theoretical Analysis

In the case of radar systems operating near OWFs, two phenomena can be distinguished that negatively affect their operation: false radar echoes and the radio shadowing. Both mechanisms are characterized in this section.

3.1. False Radar Echoes

The phenomenon of the so-called radar false echoes is generally caused by the presence of an obstacle, here the wind

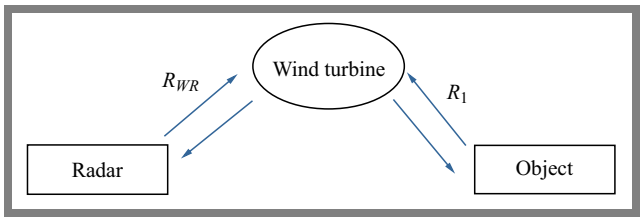

Fig. 4. False echo of the first type.

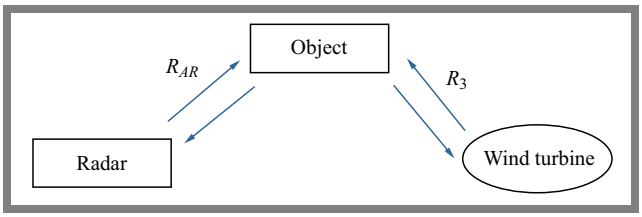

Fig. 5. False echo of the second type.

turbine, on the path between the radar and the tracked object, such as a vessel. If such obstacles are located at a sufficiently large distance from the radar, their actual influence on its operation is minor or even negligible. However, numerous scenarios exist in which false echoes can significantly disturb the visualizations generated by radars. Therefore, it is very important to be aware of that effect and analyze its scale.

Two major types of false echoes can be distinguished and the following analysis is dedicated strictly to scenarios involving wind turbines. The false echo of the first type is caused by the reflection of the radar signal from a wind turbine. If this reflected wave encounters a large object, it can be reflected to the radar, generating the false echo mentioned above. This mechanism is presented in Fig. 4.

Let P_0 represent the minimum power received by the radar, i.e. its sensitivity. For the scenario presented in Fig. 4, this parameter can be defined as follows:

$$P_0 = \frac{P_{TX} G_{TX}}{4\pi R_{WR}^2} \cdot \frac{\sigma_{TW}}{4\pi R_{WR}^2} \cdot \frac{\sigma_{TW}}{4\pi R_1^2} \cdot \frac{\sigma_{OB}}{4\pi R_1^2} \cdot \frac{\lambda^2 G_{TX}}{4\pi} \tag{24}$$

where:

P_{TX} – radar transmitter power [W],
G_{TX} – gain of the radar's transmit (and receive) antenna,
λ – wavelength [m],
σ_{TW} – radar cross section of the wind turbine [m^2],
σ_{OB} – radar cross section of the object (ship) [m^2],
P_0 – minimum received power (radar sensitivity) [W],
R_{WR} – distance between the radar and the wind turbine [m].

Let R_1 denote the maximum distance between the wind turbine and the object at which the false echo of the first type can still occur. By transforming Eq. (24), the following formula can be obtained [15]:

$$R_1 = \sqrt[4]{\frac{P_{TX} G_{TX}^2 \lambda^2 \sigma_{TW}^2 \sigma_{OB}}{P_0 (4\pi)^5 R_{WR}^4}} \,. \tag{25}$$

The next scenario is called the radar echo of the second type. This particular phenomenon can occur when the radar beam reflects from an object (vessel), and then this reflected wave reflects from the turbine and finally it "returns" back to the radar via the same object. This case is illustrated in Fig. 5.

Using the same approach as for the first type of echo, the following formula can be defined to describe the power received by the radar in the scenario presented in Fig. 5:

$$P_0 = \frac{P_{TX} G_{TX}}{4\pi R_{AR}^2} \cdot \frac{\sigma_{OB}}{4\pi R_{AR}^2} \cdot \frac{\sigma_{OB}}{4\pi R_3^2} \cdot \frac{\sigma_{TW}}{4\pi R_3^2} \cdot \frac{\lambda^2 G_{TX}}{4\pi} \,, \tag{26}$$

where R_{AR} is the distance between the radar and the object [m].

Let R_3 denote the maximum distance between the wind turbine and the object at which the false echo of the second type can still occur. Similarly to the previous scenario, this value can be obtained by transforming Eq. (26) [15]:

$$R_3 = \sqrt[4]{\frac{P_{TX} G_{TX}^2 \lambda^2 \sigma_{OB}^2 \sigma_{TW}}{P_0 (4\pi)^5 R_{AR}^4}} \,. \tag{27}$$

In order to properly apply Eqs. (25) and (27), one of the factors that needs to be determined is the radar cross section of the wind turbine σ_{TW}. In the scenarios in which Annex 1 from the ITU-R BT.1893 recommendation is applicable, this parameter will be assessed using the following formula:

$$\sigma_{TW}[\mathrm{m}^2] \approx \sigma_{TWmax}\, g^2(\theta) \,, \tag{28}$$

where σ_{TWmax} is the parameter defined by Eq. (4) and $g(\theta)$ is the function defined by Eq. (6).

If the object is located way above or way below the turbine, it is necessary to consider both horizontal and vertical planes. To do so, Eq. (28) needs to be modified in the following way:

$$\sigma_{TW}[\mathrm{m}^2] \approx \sigma_{TWmax}\, g_{ver}^2(\alpha)\, g_{hor}^2(\beta) \,, \tag{29}$$

where $g_{hor}(\beta)$, $g_{ver}(\alpha)$ are the functions defined by Eq. (6) for the horizontal and vertical plane, respectively.

It should be noted that when calculating R_1 and R_3 ranges, the σ_{TWmax} parameter may generally assume different values. As one may see from Eq. (6), the $g(\theta)$ function depends on the angle under which the transmitted signal arrives at the turbine's blade and the angle under which the reflected signal is received. Depending on the false echo type that is being considered, these will not be the same angles, because the mechanisms of these two effects are different.

In the case of a false echo of the first type, the object is the signal "transmitter" and the radar is the "receiver", whereas for the false echo of the second type, the object is both the "transmitter" and the "receiver". This observation should be taken into account when determining R_1 and R_3 values and the angles should be recalculated accordingly.

In the scenarios where Annex 2 from the ITU-R BT.1893 recommendation is applicable (radars located in close vicinity of the wind turbine), σ_{TW} is calculated using Eq. (14).

As mentioned above, correct calculation of the wind turbine's radar cross-section σ_{TW} requires, in many situations, that both the horizontal and vertical planes be taken into consideration.

For the horizontal plane, we assume that the path between the transmitter and the wind turbine is approximately perpendicular with respect to the rotor area. In such a case, the reflection from the turbine reaches the maximum level and the entire situation is considered the worst case scenario.

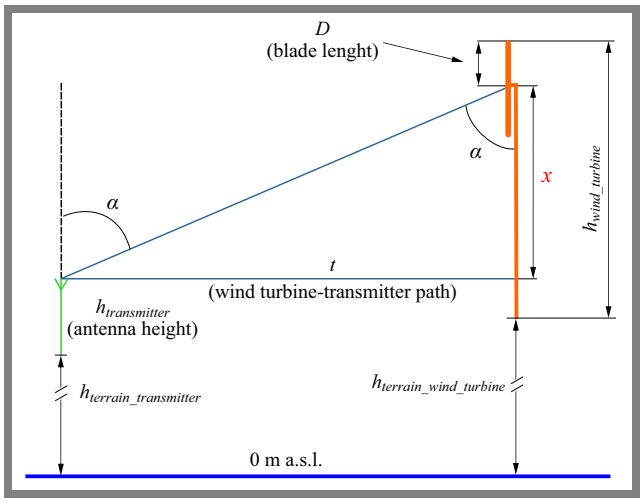

Fig. 6. Graphic interpretation of angle α.

The vertical plane is particularly important for cases in which the height of the transmitter is vastly different from the turbine's height. To obtain the angle of the transmitted signal with respect to the rotor, it is necessary to analyze the spatial configuration, including the distance between the turbine and the transmitter, the respective heights of the turbine and the transmitter and (whenever applicable) the respective terrain heights of their locations. The graphical definition of the key angle existing in such scenarios is presented in Fig. 6.

In order to calculate angle α, one needs to first obtain the value of the x section:

$$x = (h_{wind\_turbine} - D + h_{terrain\_wind\_turbine}) \\ -(h_{terrain\_transmitter} + h_{transmitter}) \ . \tag{30}$$

Using the value of x, angle α can now be calculated as:

$$\alpha = \text{arc tg}\,\frac{t}{x} \ . \tag{31}$$

Please note that strictly speaking, Fig. 6 applies to the Annex 1 model from the ITU-R Recommendation BT1893, where the electrical center of the antenna is located at the top of the rotor. In the case of the Annex 2 model, this center is located in the middle of the turbine's tower, so slight consequential modifications of both Fig. 6 and Eqs. (30) and (31) will be required for such a scenario. It should also be mentioned that Fig. 6 represents the general case and is correct for both land and offshore wind farms. For wind turbines located at sea, however, the $h_{terrain\_wind\_turbine}$ parameter is equal to zero.

3.2. Radio Shadowing

The radar transmits a short radio pulse with very high power. This pulse is focused in one direction only by the directivity of the antenna and propagates in this given direction with the speed of light. If there is an obstacle along that route, part of the energy of the pulse is scattered in all directions. A very small portion is also reflected back towards the radar. The radar's antenna receives this energy and the radar evaluates the information. All targets produce a diffused reflection, but only a limited amount of radar energy returns to the radar as a backscatter signal. The level of the reflected signal depends mainly on the object's parameters, e.g. the material it is made of, the size of the target relative to the wavelength of the radar signal, the absolute size of the target, and its shape. The target's reflectivity can be described as a radar cross-section (RCS). A higher RCS value indicates that the object can be detected more easily. Practically, the RCS of a target depends on its physical geometry and exterior features, the direction of the illuminating radar, the radar transmitter's frequency, and the electrical properties of the target's surface.

On the other hand, the maximum range of the radar R_{max} depends both on the radar transmitted power, its high sensitivity, the frequency band used and the size of the detected object (in particular its RCS), and can be calculated in the following manner [16]:

$$R_{max}\ [\text{m}] = \sqrt[4]{\frac{P_S\, G^2\, \lambda^2\, \sigma}{P_{e_{min}} (4\pi)^3}} \ , \tag{32}$$

where:

P_S – denotes the radar transmitted power in [W],
G – denotes the radar antenna gain,
λ – denotes the transmitted wave length in [m],
σ – denotes the radar cross section (RCS) of the object in [m^2],
$P_{e_{min}}$ – denotes the receiver sensitivity, i.e. the smallest received power that can be detected by the radar in [W].

Based on Eq. (32), theoretical radar range for various types of objects can be determined. It is worth noting that electromagnetic waves of higher frequencies (above 100 MHz) follow the rules of optic waves and, therefore, the radar's wave fronts also propagate in accordance with quasi-optical rules. In some cases, the Earth's curvature may prevent the radar from detecting a target, even if it is within its maximum theoretical range, which results in the presence of the so-called "blind zone". It should be noted that the radio horizon does not coincide, in practice, with the optical horizon due to the refraction of electromagnetic waves in the Earth's atmosphere. This allows radars to detect targets beyond the optical horizon and reduces the "blind zone" in which no targets can be detected.

The bending of electromagnetic waves also contributes to faults affecting distance and height measurements, but in practice such errors are eliminated by using the equivalent Earth radius instead of its actual radius. The height of the radar's antenna exerts a significant impact on radar's range, because the Earth's curvature causes flat objects to disappear very quickly behind the horizon. The maximum radar line of sight range R_{LoS} can be easily calculated using the radar antenna height and target height, according to [16]:

$$R_{LoS} = \sqrt{2\, R_{eq} H_r + H_r^2} + \sqrt{2\, R_{eq} H_t + H_t^2} \, , \tag{33}$$

where:

R_{eq} – denotes the equivalent Earth radius (taking into account standard refraction, it is equal to 4/3 of the mean Earth radius) in [km],
H_r – denotes the height of the radar antenna in [m],
H_t – denotes the height of the target object in [m].

In the case of marine radars, the formula for calculating the line of quasi-optical sight range of a radar in [km] can be

simplified to:

$$R_{LoS}\ [\mathrm{km}] \cong 4.12\left(\sqrt{H_r\ [\mathrm{m}]} + \sqrt{H_t\ [\mathrm{m}]}\right) . \tag{34}$$

Obstacles within the radar coverage area also have a different effect on the radar's range. Unlike optical waves, which are obscured by obstacles present along the line of sight, electromagnetic waves may be able to penetrate some of such obstacles. This ability depends, of course, on the object's material. In the case of offshore wind turbines, their influence on radar ranges depends on the distance between the radar antenna and the turbines. When the radar transmitter is in the vicinity of the turbine, according to Annex 2 to the ITU-R BT.1893-1 [2] model, the reflection from the turbine is caused primarily by its mast. Due to the fact that the mast is usually made of concrete and steel, it can be assumed that it constitutes an insurmountable barrier (obstacle) to the radar wave, and the radar signal no longer propagates behind the turbine. On the other hand, for long distances between the radar and the turbine, according to Annex 1 to the ITU-R BT.1893-1 model [2], the reflection is caused primarily by the wind turbine's blades which are made of fiberglass-reinforced polymer. In that case, the turbine reflects and absorbs only some of the electromagnetic wave energy and most of the radar signal continues to propagate behind the turbine. In both cases (near-field and far-field scenarios), suitable mathematical formulas are used to calculate the effective reflecting surface of the wind turbine (RCS), depending on the distance between the radar and the wind turbine. In the near-field scenario, RCS is calculated based on the turbine mast's parameters and in the far-field scenario – the wind turbine rotors are taken into account – as explained in the previous sections of the paper.

For the purpose of this article, the radar ranges (signal propagation) in the presence of the offshore wind farms have been simulated using a professional simulation tool developed by the authors. The simulations have been conducted using the newest, general purpose ITU-R P.2001-4 propagation model [17] which, by definition, is very universal and applicable to numerous types of terrestrial radio systems operating within the 30 MHz to 50 GHz frequency range. It is suitable for a wide range of frequencies, distances, and percentage times, with no discontinuities in its output. It allows, in particular, to predict both fading and amplification of signal levels, for signals which may be either desired or potentially interfering. The propagation model utilizes a digital terrain model and, additionally, allows to model the presence of terrain obstacles. In the case of offshore wind turbines, it is necessary to correctly model the area in which turbines are located and take into account their specific impact on increasing propagation attenuation.

4. Simulation Methodology

In order to examine the impact of OWFs on radar systems, a list of examples of currently used and planned wind turbines was prepared (Tab. 1) and two of them were selected for comparative research. Turbine parameters that could not be found in open-access specifications were estimated on the basis of the following equations.

The total area of the blades may be calculated using the quality number coefficient Q [18], [19] which determines the efficiency of energy production by the rotor. It is a ratio of the rotor swept area to the total area of the material needed to build this rotor.

A typical, 3-bladed, horizontal axis rotor has a Q equal to 31.25 [18], [19].

Consequently, the total area of three blades A can be calculated using the expression [18], [19]:

$$A = \frac{P}{Q} = \frac{P}{31.25} , \tag{35}$$

where P is the rotor swept area [m^2], approximately expressed as:

$$P = \pi R^2 , \tag{36}$$

where R stands for the rotor radius [m].

The rotor radius is approximately[1] equal to the blade length D.

Finally, by substituting Eq. (36) into (35), the total area of the blades A can be expressed as:

$$A = \frac{\pi R^2}{31.25} . \tag{37}$$

In order to calculate blade width at the hub S_{max} – under the assumption that the blades are approximately triangular – the following formula may be used:

$$S_{max} = \frac{2\,A}{3\,R} . \tag{38}$$

Mean width of a blade S is:

$$S = \frac{S_{max}}{2} . \tag{39}$$

In Tab. 1 the parameters of yellow-marked turbines have been used in the simulations described in the remaining part of the article. For brevity, these turbine types will be referred to as legacy and modern turbines. In order to analyze the impact of offshore wind farms on radar signals, the following scenarios have been taken into consideration.

Within an area of 10 × 10 km, at sea, two variants of the turbines' arrangements characterized by different densities were established:

- 5 × 5 – 25 turbines at 2 km intervals (see Fig. 7a) ,
- 10 × 10 – 100 turbines at 1 km intervals (see Fig. 7b).

In order to simulate an offshore wind farm located in the Polish Exclusive Economic Zone in the Baltic Sea, two locations of radar stations have been established. The first one represents a coastal radar on the Polish shoreline, positioned 12 NM (nautical miles) from the wind farm – Fig. 7. The distance of 12 NM (22.2 km) from the shore was selected because it represents the boundaries of the Polish territorial waters. According to Polish law, offshore wind farms can only be built beyond that mark, i.e. at least 12 NM from the shore.

[1] This is merely an approximation, because the rotor swept area is calculated with respect to the middle of the rotor. This middle point is not exactly at the beginning of the blade, but rather in the middle part of the hub. The size of the hub determines the error of this approximation.

Tab. 1. List of examples of operational and planned wind turbines.

	Turbine power	Tower height [m]	Tower radius [m]	Rotor diameter [m]	Blade length [m]	Max blade width [m]	Average blade width [m]	Surface area of a single blade [m^2]	Total blade surface area [m^2]	Speed range [rpm]	RCS for the rotor [dBm^2] 3/10 GHz	RCS for the rotor taking into account the reflection wave coefficient [dBm^2] 3/10 GHz	RCS for the tower [dBm^2] for 12 NM
Non-modern onshore turbines	2 MW	100	3	90	45	3.0	1.5	67.9	203.6	9–19	77.2 / 87.6	68.2 / 78.6	45.4
Current onshore turbines	3.3/3.45 MW	117/137	3	126	61.7	4.0	2	123.4	370.2	5.9–16.3	82.4 / 92.8	73.4 / 83.8	45.4
	3.45 MW	134	3	132	64.5	4.32	2.16	139.4	418.2	10.9	83.4 / 93.9	74.4 / 84.9	45.4
Current "legacy" offshore turbines	5.28 MW	90	3.1	122	59.5	3.99	2	118.6	355.9	8	82 / 92.5	73 / 83.5	45.6
	6 MW	102	3.1	154	75	5.03	2.52	188.5	565.5	11	86 / 96.5	77 / 87.5	45.6
	7 MW	110	3.1	154	75	5.03	2.52	188.5	565.5	11	86 / 96.5	77 / 87.5	45.6
	8.4 MW	110	3.1	167	81.4	5.46	2.73	222	666.1	12	87.5 / 97.9	78.5 / 88.9	45.6
	12 MW	150	3.2	220	107	7.17	3.59	383.7	1151	7	92.2 / 102.7	83.2 / 93.7	45.7
Modern offshore turbine	14 MW	143–147	3.25	236	115	6.5	3.25	373.75	1121.25	7.8–8	92 / 102.4	83 / 93.4	45.8
	14 MW	138	3.4	220	107	7.0	3.5	374.5	1123.5	8	92 / 102.5	83 / 93.5	46.0
Future offshore turbine	17.85 MW	147	3.5	250	122	6.6	3.3	402.6	1207.8	4.2–7.8	92.6 / 103.1	83.6 / 94.1	46.1
Note: values in blue are estimated using formulas (35)–(39)													

Tab. 2. General simulation scenarios.

Scenario number	Distance between radar and wind farm [NM]	Dominant reflecting element of the turbine	RCS of the wind turbine (tower/rotor) [dBm^2]*	Radar						Target		
				Type	Frequency band	Power [dBm]	Antenna gain [dBi]	Antenna height [m]	Sensitivity [dBm]	Type	RCS [m^2]	Height [m a.s.l.]
1	2	Tower (Annex 2)	45.6	Ship radar	S	70	28	10	–97	Small vessel	4	4
2					X	70	29	10	–98	Large vessel	120	10
3					X	70	29	10	–98	Small vessel	10	4
4					X	70	29	10	–98	Large vessel	300	10
5	12	Rotor (Annex 1)	73	Coastal radar	S	75	33	50	–108	Small vessel	4	4
6					S	75	33	50	–108	Large vessel	120	10
7			83.5		X	74	33	50	–98	Small vessel	10	4
8					X	74	33	50	–98	Large vessel	300	10
9	2	Tower (Annex 2)	45.8	Ship radar	S	70	28	10	–97	Small vessel	4	4
10					S	70	28	10	–97	Large vessel	120	10
11					X	70	29	10	–98	Small vessel	10	4
12					X	70	29	10	–98	Large vessel	300	10
13	12	Rotor (Annex 1)	83	Coastal radar	S	75	33	50	–108	Small vessel	4	4
14					S	75	33	50	–108	Large vessel	120	10
15			93.4		X	74	33	50	–98	Small vessel	10	4
16					X	74	33	50	–98	Large vessel	300	10
Note: RCS for the rotor takes into account the reflection wave coefficient (9 dB)												

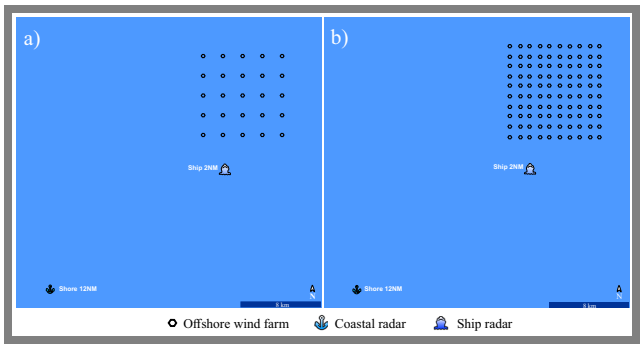

Fig. 7. Coastal and vessel-borne radar locations for simulations concerned with 5 × 5 a) and 10 × 10 b) turbine configurations.

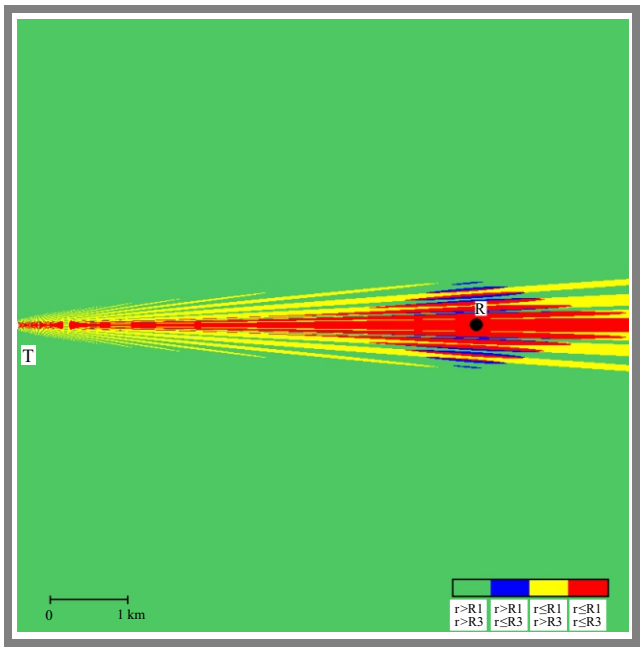

Fig. 8. Example visualization of false radar echoes obtained using the software tool.

The second location represents an example position of a vessel-borne radar located 2 NM from the wind farm (Fig. 7). This distance of 2 NM (3.7 km) corresponds to the mandatory separation between wind farm boundaries and maritime traffic routes (e.g. traffic separation schemes), as required by the authorities for all Polish offshore wind farms. The general simulation scenarios on which the analysis is based are presented in Tab. 2. The specific scenarios were selected to be able to compare the impact of the following elements on the obtained results:

- distance between the radar and the wind farm: 2 NM for the vessel-borne radar and 12 NM for the coastal radar,
- radar frequency band: S and X,
- target type: small and large vessels.

Additionally, for the purpose of investigating the radio shadowing effect, each simulation scenario has been conducted twice, for different offshore wind farm configurations. In order to distinguish the results obtained for both scenarios, the following notations were introduced: scenario XA and XB, where X represents a scenario number from Tab. 2, A denotes the 5 × 5 turbine configuration with the distance between the turbines equaling 2 km, and B represents the 10 × 10 turbine configuration with the distance between the turbines amounting to 1 km.

4.1. False Radar Echo Simulation Methodology

The analysis of false radar echoes was carried out using a dedicated software tool developed by the authors of this paper. The tool allows to visualize the areas around the wind turbine and around the radar where false echoes of the first and second types may occur.

As we explained earlier, the false echo of the first type is caused by the reflection of the radar wave from the wind turbine. If this reflected wave encounters a large object (a vessel), it can be reflected back to the radar, thus generating this type of echo. The false echo of the second type occurs in a situation where the radar beam reflects from an object, and this reflected wave reflects once again from the turbine and "returns", via the same object, to the radar.

The risk of false echo occurring is limited to certain distances between the vessel and the wind turbine (and those distances vary for different types of echoes). The tool allows to verify whether the distance from the vessel to the turbine (given the arrangement of these elements and the radar) is sufficient to eliminate the possibility of false echoes materializing.

The basic concept of this tool can be described as follows. After entering all the relevant parameters of the wind turbine, the radar and defining the size of the area covered by the analysis, i.e. a square with the dimensions of its side defined by the user, the simulation can be initiated. It is assumed that the wind turbine is always located at a fixed position – exactly halfway along the left edge of the analysis area.

The position of the radar is defined by the user who specifies the distance between the radar and the wind turbine and the angle of the radar with respect to the turbine. Finally, the position of the object, essential for the phenomenon of false echoes, is variable. In each iteration, the object is located at a different point within the analysis area. It is assumed that the resolution of the analysis area is 800 × 800 points, so the entire simulation "scans" 640,000 potential locations of the object.

In each iteration, the software tool calculates the distance between the object located at the current point of the analysis area and the turbine. Then, it verifies whether it is greater than the theoretical values of R_1 and R_3 distances or not – see Eqs. (25) and (27). If it is indeed greater than either R_1 or R_3, it means the vessel is so far away from the wind turbine that it most likely will not cause any false echoes. If the distance is less than R_1 or R_3, however, the false echo is likely to occur. The visualization generated by the tool relies on the following color scheme to denote the relevant events:

- green – the distance between the ship and the turbine for the given ship's location is greater than R_1 and greater than R_3 (neither the false echo of the first type, nor the second type occurs),

- blue – the distance between the ship and the turbine for the given ship's location is greater than R_1 and less than R_3 (the false echo of the first type does not occur, but the false echo of the second type does),
- yellow – the distance between the ship and the turbine for a given ship's location is less than R_1 and greater than R_3 – (the false echo of the first type occurs, but the false echo of the second type does not),
- red – the distance between the ship and the turbine for a given ship's location is less than R_1 and less than R_3 (false echoes of both the first type and the second type occur simultaneously).

An example of the visualization generated in the tool can be seen in Fig. 8. It was obtained for the analysis area of 8 × 8 km and the distance between the wind turbine and the radar of 6 km. "T" denotes the fixed position of the wind turbine and "R" represents the location of the radar.

The simulation of false echoes has been performed for the scenarios presented in Tab. 2.

It has to be noted that false echoes are always calculated for a specific orientation of the radar and the wind turbine. Therefore, unlike radio shadowing analysis, these simulations do not apply to scenarios in which multiple turbines are present at each site, but are carried out with respect to a single wind turbine located at a predefined location. In light of the above, the number of scenarios is lower compared to those evaluated in the course of radio shadowing investigations (see Tab. 2), even though they are based on exactly the same parameters of the wind turbine and of the tracked object.

The simulations were performed for a coastal radar operating in S and X bands and a vessel-borne radar (S and X bands). In the case of simulations focusing on coastal radars, the assumed distance between the radar and the wind turbine is 12 NM (approx. 22.2 km), while in the case of vessel-borne radars, this distance is 2 NM (approx. 3.7 km). The angle between the rotor plane and the turbine-radar section is constant and set at 90° for every simulation. For the analyzed scenarios, two types of tracked objects: a large vessel (high RCS) and a small vessel (low RCS) [20], [21] and two types of wind turbines: a current "legacy" turbine (smaller dimensions, scenarios 1–8) and a modern turbine (larger dimensions, scenarios 9–16) were taken into consideration. A detailed list of the scenarios and their respective parameters is presented in Tab. 2.

4.2. Radio Shadowing Simulation Methodology

The radio planning tool has been adjusted to calculate active radar ranges in different bands (S and X) and to take into account parameters of the selected radar object (RCS). In simple terms, radio signal transmitted by the radar is reflected by the detected object and returns to the radar's receiver. The radio planning tool normally can simulate only one direction of propagation, therefore the edge of the radar range (allowing detection the object with specified RCS and reception its reflected signal at the radar location) has to be defined. In the first step, for a defined object and its RCS, the maximum radar range R_{max} is calculated based on Eq. (32). Next, assuming a direct line of sight between the radar transmitter and the target, free space loss $FSPL$ is calculated for this range, based on the simplified formula given below [22]:

$$\begin{aligned} FSPL\ [\mathrm{dB}] = 20\log(R_{max}\ [\mathrm{km}]) \\ +20\log(f\ [\mathrm{MHz}]) + 32.44\ , \end{aligned} \tag{40}$$

where f denotes radar frequency.
In the next step, using the radar's parameters, such as transmitted power P_S, antenna gain G and free space loss $FSPL$, the level of the signal received at the terminal of an isotropic antenna P_e [dBm] at the edge of the radar's range is calculated:

$$P_e\ [\mathrm{dBm}] = P_S\ [\mathrm{dBm}] + G\ [\mathrm{dBi}] - FSPL\ [\mathrm{dB}]\ . \tag{41}$$

The obtained signal level P_e represents the smallest signal on the edge of the radar range which, after reflection from the object's surface and its transmission back to the radar, can be detected at the radar receiver's sensitivity level of $P_{e_{min}}$. In the course of a subsequent analysis that takes into account the relationship between the detected object's radar cross section (RCS) and the isotropic antenna's effective area, surface power density of the received signal in [dBmW/m^2] will be calculated and presented.

Once the level of the signal received at the edge of the radar range is established, propagation analysis may be simulated. Due to long radar ranges in maritime environments, often exceeding radio horizon range, Earth curvature is the primary factor affecting signal propagation, being the main obstruction within the first Fresnel zone and causing significant signal attenuation, even if the apparent line-of-sight signal path is not blocked. Due to diffraction, the simulated active radar ranges will be shorter than both the maximum range R_{max} Eq. (32) and the maximum line of sight range R_{LoS} Eq. (34). Table 3 presents the calculations of radar ranges taken into consideration by the authors of this article.

In the course of the simulations, the presence of offshore wind turbines within active radar areas was modelled as a group of obstacles introducing the radio shadowing effect. The shape of each turbine (obstacle) was defined as a regular hexagonal prism, to correspond to a worst-case scenario, assuming that the turbine rotor was rotating in an arbitrary direction. Depending on the distance between the radar and the turbines, different prism dimensions and signal attenuation factors have been used. As mentioned above, in the case of long distances between the radar and the turbine, wind turbine blades (made of fiberglass reinforced polymer) are the primary components responsible for signal reflection and radio shadowing. In this case, the dimensions of the prism modelling the turbine are as follows: the length of the prism's side is equal to the radius of the turbine's rotor (half of the rotor's diameter) and its height is equal to the total height of the turbine. Degradation of radar signal after passing through the turbine area can be calculated using the previously mentioned mismatch loss parameter (ML, equaling approx. 0.6 dB) Eq. (13). Taking into consideration the fact that the radar signal follows the same propagation route twice (from radar to the object and back), it is attenuated by the

Tab. 3. Radar range summary.

Radar type	Coastal				Vessel-borne			
Radar band	S band		X band		S band		X band	
Frequency [MHz]	3200		9400		3200		9400	
Transmitted power P_S [dBm]	75		74		70		70	
Radar antenna gain G [dBi]	33		33		28		29	
Radar antenna height H_r [m a.s.l.]	50		50		10		10	
Radar receiver sensitivity $P_{e_{min}}$ [dBm]	–106		–98		–97		–98	
Radar object type	Small vessel	Vessel	Small vessel	Vessel	Small vessel	Vessel	Small vessel	Vessel
RCS σ [m^2]	4	120	10	300	4	120	10	300
Height of the target H_t [m a.s.l.]	4	10	4	10	4	10	4	10
Radar maximum range R_{max} [km]	97.1	227.2	42.4	99.3	24.4	57.1	18.9	44.3
Radar maximum LoS range R_{LoS} [km]	37.4	42.2	37.4	42.2	21.3	26.1	21.3	26.1
Simulated active radar range [km]	29.3	41.0	28.8	38.4	9.8	18.1	12.3	20.1

wind turbine twice. Therefore, the attenuation factor for the turbine areas takes into account a double mismatch loss value adjusted for the size of turbine modeling prisms. This factor has been introduced to the propagation model for further simulations, as an additional signal attenuation caused by offshore wind turbines affecting the radar signal. In the case of small distances between the radar and wind turbine, the mast (usually made of concrete and steel) plays a key role. In that case, the dimensions of the prism modelling the turbine (mast) are: the side length of the prism is equal to the mean turbine mast radius (half of the mean mast diameter) and its height is equal to the height of the turbine's mast. For the purpose of further simulations, it is assumed that the mast blocks the radar wave behind the turbine.

Figure 9 shows how wind turbine areas were modeled and Tab. 4 presents the parameters taken into account during subsequent simulations. Figure 10 presents examples of propagation paths passing through the wind farm area for coastal radar scenarios (S and X band radars), visualizing the obstruction of the first Fresnel zone by the Earth's curvature and the wind turbines.

5. Simulation Results

This section presents the results of simulation tests performed for the scenarios described in Section 4. We begin by discussing the nature of the unwanted signal reflected from the turbine's rotor (Annex 1) and turbine's mast (Annex 2). After that, the simulation results are presented and are analyzed for false radar echoes and the radio shadowing effect.

5.1. Characteristics of Unwanted Signal Reflections from the Turbine

As explained in the previous sections, one of the main factors generating false radar echoes is the reflection of the radar signal from the wind turbine. It is therefore worthwhile to discuss the nature of this reflection for the two relevant scenarios:

- reflection from the rotor (in which case the Annex 1 model is applicable),
- reflection from the turbine's tower (Annex 2).

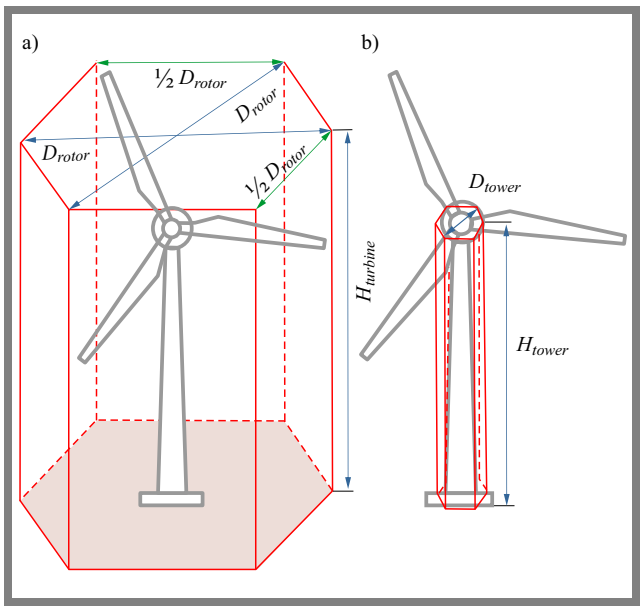

Fig. 9. The method modelling wind turbines as terrain obstacles for radio shadowing analysis: a) for large distances between the radar and the turbine – the coastal radar scenario, b) for radars located in the vicinity of the turbine – the vessel-borne radar scenario.

Tab. 4. Parameters of offshore wind turbine modelling areas.

Radar–turbine distance	Large distance			Short distance		
Prism dimensions	Prism side length	Prism height	Signal attenuation	Prism side length	Prism height	Signal attenuation
Legacy offshore turbine	61 m	151 m	9.8 [dB/km]	3 m	90 m	Blocking
Modern offshore turbine	118 m	263 m	5.1 [dB/km]	3 m	145 m	Blocking

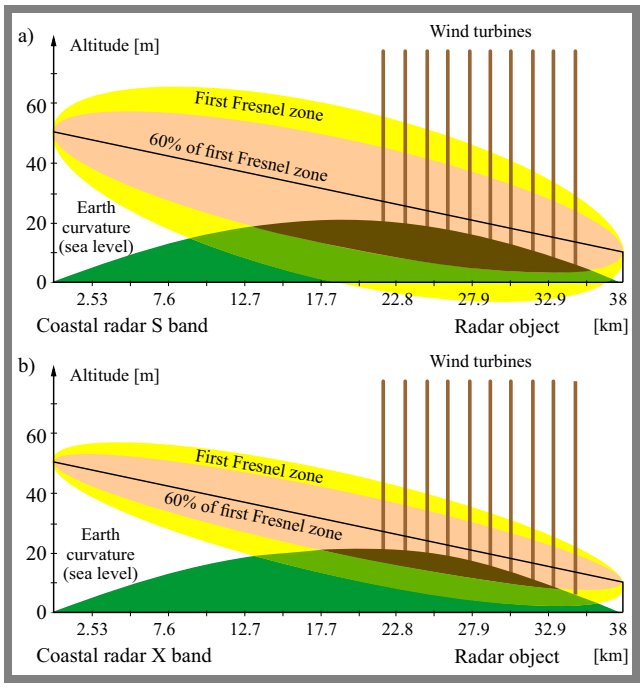

Fig. 10. Visualization of obstructions of the first Fresnel zone created by wind turbines along one of the propagation paths for coastal radar simulations for a) S band and b) X band.

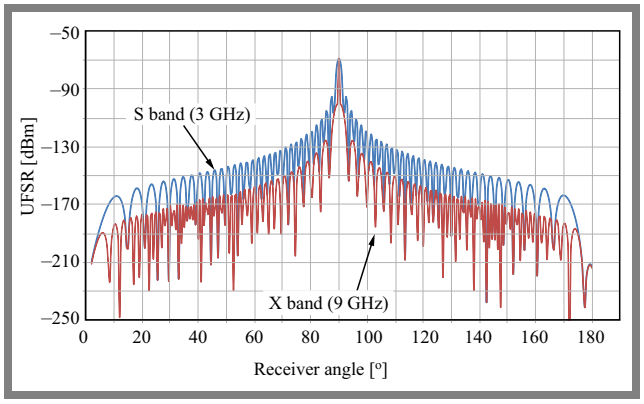

Fig. 11. UFSR vs. receiver angle for S band (3 GHz) and X band (9 GHz) radars calculated using the ITU-R BT.1893-1 Annex 1 model (reflection from the turbine's rotor).

The formulas describing the unwanted (reflected) signal level, UFSR, for the two Annexes, have already been provided – see Eqs. (20) and (22). Based thereon, the characteristics of this parameter, as a function of the receiver angle, have been established and presented below for two typical radar frequencies: 3 GHz (S band) and 9 GHz (X band). Figure 11 illustrates the level of the unwanted signal vs. receiver angle

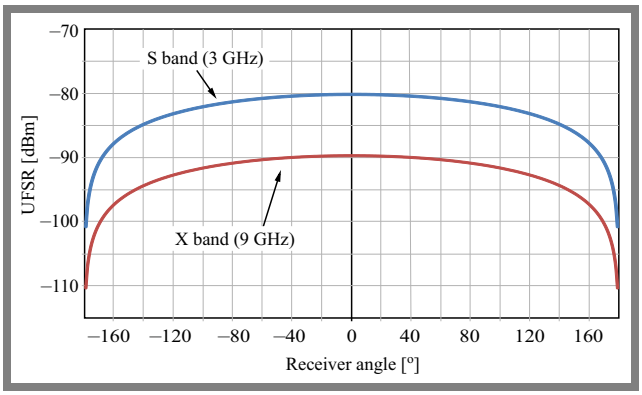

Fig. 12. UFSR vs. receiver angle for S band (3 GHz) and X band (9 GHz) radars calculated using the ITU-R BT.1893-1 Annex 2 model (reflection from the turbine's tower).

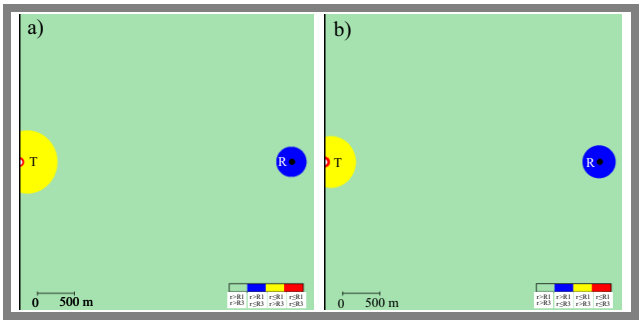

Fig. 13. False echoes for a vessel-borne radar (Annex 2), a current (legacy) wind turbine and a large vessel: a) S band radar (scenario 2), b) X band radar (scenario 4). Area of analysis: 4 × 4 km ("T" – location of the wind turbine, "R" – location of the radar).

for the Annex 1 model and Fig. 12 depicts the corresponding relation for the Annex 2 model. The simulation parameters are as follows:

- For Annex 1 simulations: EIRP of the radar 75 dBm (includes the antenna gain), distance between the transmitter and the wind turbine 10 NM (22.2 km), distance between the wind turbine and the receiver 10 NM (22.2 km), transmitter angle with respect to the rotor 90° (maximum reflection), maximum chord of the wind turbine blade 6.5 m, total area of the blades 1121.25 m^2.
- For Annex 2 simulations: EIRP of the radar 70 dBm, distance between the transmitter and the wind turbine 2 NM (3.7 km), distance between the wind turbine and the receiver 2 NM (3.7 km), horizontal transmitter angle with respect to the tower 0°, radius of the wind turbine tower 3.1 m. Parameters of the rotor are not relevant for the Annex 2-related analysis.

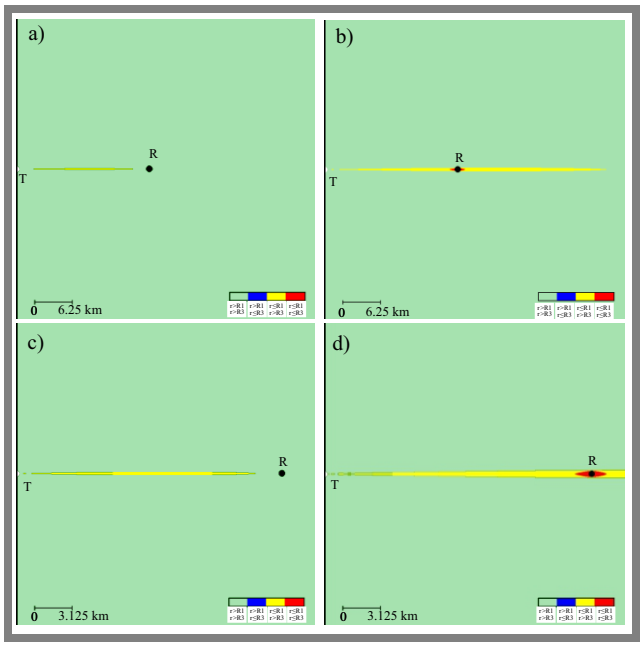

Fig. 14. False echoes for an S band coastal radar (Annex 1), a "modern" wind turbine and: a) a small vessel (scenario 13), b) a large vessel (scenario 14). Area of analysis: 50 × 50 km. Illustrations c) and d) are identical to a) and b) respectively, but feature a smaller analysis area: 25 × 25 km. ("T" – location of the wind turbine, "R" – location of the radar).

As one can see, the two different reflection mechanisms result in two completely different characteristics of the UFSR parameter. In the case of the reflection from the rotor (Annex 1) shown in Fig. 11, numerous alternating minimums and maximums of the reflected signal power can be observed. The number of those minimums/maximums increases as the frequency becomes higher, which is evident from the figure. If the same characteristics applied to much lower frequencies, e.g. in the VHF/UHF band, the resulting curve would only contain a few "side lobes", but the general relation between the number of lobes and the frequency would still hold.

On the other hand, we can observe that for a lower frequency (3 GHz), the level of the unwanted reflected signal is visibly higher than for 9 GHz. It may seem surprising at a first sight, as the reflection coefficient ρ is inversely proportional to the wavelength and directly proportional to frequency – see Eq. (21). UFSR, however, depends not only on ρ, but also on the attenuation level on the path between the wind turbine and the receiver, which obviously takes greater values as the frequency goes up. In many scenarios, the attenuation component[2] will overcome the ρ-related component, which results in a higher level of the reflected signal observed at lower frequencies. The absolute maximum of UFSR for the Annex 1 case occurs when the transmitter angle is equal to the receiver angle (here 90°).

The analysis carried out for the Annex 2 scenario, where reflection from the turbine tower is the dominant reflection mechanism, resulted in characteristics that differ considerably from those presented above. The first aspect we need to observe is that, in this case, the frequency does not affect the shape of the UFSR curve. To explain this, we need to examine closely the Annex 2 formula for RCS – see Eq. (14).

Theoretically, it is a function of wavelength, but a simple mathematical simplification of this equation shows that λ cancels out, so ultimately the Annex 2 RCS does not depend on the frequency. The nature and shape of the curve is not surprising either. The reflection from the tower is obviously much more straightforward and "simple" scenario compared to the reflection from constantly rotating triangular turbine blades. Consequently, the received reflected signal simply decreases as the receiver moves away from the tower, with no local minimums/maximums observed.

Please note that, generally speaking, a wind turbine may be considered to be an "antenna" radiating the reflected signal around it. The characteristics presented in Figs. 11 and 12 can be interpreted as the patterns of such a peculiar type of an "antenna", which is a very useful observation for the actual analysis on the wind turbines' impact of radiocommunication systems.

5.2. False Radar Echoe Simulation Results

The results of false echo simulations have been summarized in Tab. 5. The table shows the maximum observable ranges of false echoes, their shape and maximum angular width for each of the considered scenarios.

The limited length of this article does not allow us to present all the results in a graphic form, so we can only include a few exemplary simulations. In Fig. 13, the characteristics of false echoes for a vessel-borne radar (Annex 2) and a current (legacy) wind turbine have been presented. The tracked object is, in this case, a large vessel. Figure 13a contains the simulation results for S band radar (Scenario 2), whereas Fig. 13b presents the outcomes for X band radar (Scenario 4). The simulations have been performed for an area of 4 × 4 km.

Figure 14 presents the characteristics of false echoes for a coastal S band radar (Annex 1) and a "modern" wind turbine. In part a) of this illustration, the tracked object is a small vessel (Scenario 13) and in part b) the tracked object is a large vessel (Scenario 14). The simulations have been performed for an area of 50 × 50 km. Additionally, part c) and d) include the same simulations as in part a) and b), but performed on a smaller scale (25 × 25 km) to improve clarity and to better illustrate the situation around the radar.

Based on the obtained results, the following conclusions can be drawn regarding the false radar echo phenomenon. In the case of coastal radars (analyzed using the Annex 1 model), the potential range of the false echoes is affected by:

- distance between the radar and the wind turbine: the greater it is, the shorter the false echo ranges,
- radar cross section of the object (e.g. vessel) – in this case the relationship is directly proportional: significant cross section of the object will inevitably result in stronger and more troublesome false echoes,

[2] which was simulated, in this case, using the free-space loss model

Tab. 5. Results of false echo simulations (scenario numbers correspond to Tab. 2).

Scenario	Maximum range of the false echo: T – from the turbine, R – from the radar	False echo of the first type	False echo of the second type	Shape of the false echo	Maximum angular width of the false echo [°]
1	≈160 m (T)	Yes, dominant	Not present	Circular	360
2	≈520 m (T), ≈220 m (R)		Minor, around the turbine and radar	Circular	360
3	≈130 m (T)		Not present	Circular	360
4	≈480 m (T), ≈240 m (R)		Minor, around the turbine and radar	Circular	360
5	≈6.3 km (T)		Not present	Narrow beam	4
6	≈14.9 km (T), ≈800 m (R)		Minor, around the radar	Narrow beam	4
7	≈7.3 km (T)		Not present	Very narrow beam	2
8	≈16.8 km (T), ≈650 m (R)		Minor, around the radar	Very narrow beam	2
9	≈160 m (T)		Not present	Circular	360
10	≈530 m (T), ≈220 m (R)		Minor, around the turbine and radar	Circular	360
11	≈140 m (T)		Not present	Circular	360
12	≈440 m (T), ≈250 m (R)		Minor, around the turbine and radar	Circular	360
13	≈20.1 km (T)		Not present	Narrow beam	4
14	≈46.8 km (T)		Minor, around the radar	Narrow beam	4
15	≈22 km (T)		Not present	Very narrow beam	2
16	≈51 km (T), ≈1 km (R)		Minor, around the radar	Very narrow beam	2

- physical dimensions of the turbines, particularly their rotors – again, the relationship is proportional: large rotors translate into stronger reflection capabilities of the turbine and, thus, into a greater range of the unwanted false echo effects.

In our analysis, we considered two types of wind turbines, referred to as "current" (smaller) and "modern" (larger) turbines. In the case of the S band radar (3 GHz), the calculated maximum ranges of the false echoes were between 6.3 km ("legacy" turbine, object with low RCS) and 46.8 km (modern turbine, object with high RCS). In the case of the X band radar, the maximum ranges were between 7.3 km and 51 km, respectively. With that taken into consideration, it may be argued that the range of this phenomenon is, in some cases, significant. While it is theoretically true, there are a few very important observations to make.

Firstly, all the simulations in this section of the article were conducted for the worst-case scenario, where the angle between the rotor plane and the turbine-radar section is 90°.

Under such an assumption, the reflection from the turbine is maximized, as is the radar cross section (RCS) of the turbine. In fact, in this case RCS is several magnitudes of order greater than the actual, physical area of the turbine's rotor. Consequently, the ranges of the false echoes presented here are the absolute theoretical maxima of this phenomenon.

The probability that the exact conditions required for the maximum reflection will be satisfied in realistic scenarios is rather low. So, in the majority of cases, the actual impact of the false echoes will be much lower and sometimes even negligible.

Secondly, the Annex 1 false echoes – despite their range – generally occur within very narrow angular ranges. They are slightly wider for S band radars (maximum width of approx. 4°), whereas for X band radars, they do not exceed 2°. This means that an object (vessel) that is necessary for the false echo to occur will remain in that area for a very short period of time, which substantially reduces the actual impact of such a phenomenon. This observation would be even more relevant in the case of aeronautical objects (helicopters, planes) whose speed is obviously significantly greater than the speed of a vessel.

As we can also notice, false echoes of the first type (marked yellow) are generally dominant across all simulations. On the other hand, the characteristics of large vessels (high RCS of

the tracked object) often feature small areas of false echoes of the second type located around the radar's locations (they are marked blue or – when they coincide with the false echo of the first type – red).

The comparison of the formulas for the maximum ranges of the false echoes, R_1 and R_3, provides an explanation for this. It is evident that R_3 depends, to a larger extent, on the R_{CS} of the object in question than R_1 (R_3 is proportional to σ_{OB}^2, while R_1 is only proportional to σ_{OB}). Therefore, if the scenario involves a large object, the probability of the false echo of the second type occurring alongside echoes of the first type is much higher.

For the purpose of the simulations, the parameters of the reflecting objects – particularly their RCSs – have been selected to take into account the operational frequencies of the radar, so a large vessel in the S band features a smaller RCS than in the X band. The same relation is true for a small vessel. Consequently, false echoes are comparable for X and S band radars if the remaining simulation parameters are the same.

In this context, the word "comparable" should be interpreted denoting a difference between the false echo ranges for X and S band radars not exceeding a few kilometers, and the echoes for X band radars being slightly longer than those calculated for lower radar frequencies. Please note that if the RCSs of the reflecting object were identical for the two frequencies, the expected false echoes would be longer for the S band radar which is characterized by a higher wavelength that the X band, since the mathematical formulas for R_1 and R_3 are directly proportional to λ.

The simulations conducted for vessel-borne (on-board) radars resulted in significantly different results than those discussed above. Due to the relatively short distance between the on-board radar and the wind turbine (equaling only 2 NM, as opposed to 12 NM assumed for simulations concerned with coastal radars), it was necessary to apply Annex 2. The radar cross section of the wind turbine calculated in compliance with that Annex is substantially smaller than the Annex 1-based RCS, which translates into much shorter ranges of the false echoes (hundreds of meters rather than kilometers). The nature of the false echoes themselves is very different as well.

As one may recall, in Annex 2, the reflection from the turbine's tower (mast) is the most dominant effect. Consequently, the false echoes cover the full angular area around the turbine and the radius of that area can be obtained directly from the R_1 and R_3 formulas introduced earlier in the article. The nature of these false echoes is also consistent with the reflection characteristics presented earlier in the paper (Fig. 12).

Similarly to the previous simulations, two types of the wind turbine (referred to as a "current" turbine and a "modern" one) were considered for Annex 2. In the case of an S band vessel-borne radar (3 GHz), the calculated maximum ranges of the false echoes were between 160 m ("current" turbine, object with low RCS) and 530 m ("modern" turbine, object with high RCS). In the case of an X band vessel-borne radar, the maximum ranges were between 130 m and 480 m, respectively.

Again, false echoes of the first type were clearly the most dominating effect across all simulations. However, for the scenarios involving a large vessel, noticeable areas affected by the false echoes of the second type could also be observed. The explanation of that effect, provided earlier in this section, remains valid for simulations concerned with vessel-borne radars as well.

Despite the fact false echoes can theoretically affect a significant area around the wind turbine (in the case of coastal radars their ranges can exceed dozens of kilometers), no corrective actions are recommended in this case. First of all, false echo is a phenomenon of a very dynamic nature. It depends on the current locations of the radar and wind turbines with respect to additional reflecting objects (in this case – usually a vessel). Since this object is usually in motion, spatial arrangements of the three entities mentioned above are constantly changing, and so are the characteristics and severity of the false echoes.

In the case of the analysis related to a vessel-borne radar (Annex 2), not just one but two entities in motion are involved: the object and the radar itself, located on board of another vessel, which makes this scenario even more dynamic and unpredictable. Consequently, it is often the case that a specific temporal arrangement of the entities results in significant false echoes, but a few moments later, when this arrangement changes, the severity of the phenomenon becomes substantially lower.

The most common corrective measure applied to compensate the impact of wind farms on radar systems consists in installing an additional corrective radar at a location selected to maximally mitigate the negative effect. As explained above, however, in the case of false echoes, such an approach would not make much sense. It is impossible to select the location of such a corrective radar to make sure that it would be able to compensate for the negative effect throughout the entire affected area. Such a radar would work for one specific arrangement of the turbine/radar/vessel only and would be totally ineffective for other scenarios. On the other hand, the inability to physically compensate for the false echoes surely does not constitute a substantial obstacle in the development of offshore wind farms. This stems from the following reasons:

- As mentioned above, even though theoretical range of false echoes for coastal radars (Annex 1) can be very high, their angular width is actually very low (2–4°), so their actual impact on the operation of radars is mostly negligible. Also, all the simulations described in the paper were conducted to address "the worst case scenario", i.e. the case of a maximum possible reflection from the wind farm. It is extremely unlikely that such a maximum reflection will be occurring regularly in practice.
- The range of theoretical false echoes for vessel-borne radars (Annex 2) cover nearly the entire angular space around the turbine (and sometimes around the radar), but their ranges, in turn, are relatively short (hundreds of meters). For most offshore wind farm projects, some kind of a protection zone may be established, e.g. 2 NM around the farm, and

Tab. 6. Results of coastal radar simulations.

Scenario number	Turbine configuration	Turbine type	Radar type	Target type	Nominal radar range [km]	Max radar range reduction		Affected radar area [km^2]
						[km]	[%]	
5A	5 × 5	Legacy	S band	Small vessel	29.33	1.86	6.3%	1.3
6A	5 × 5	Legacy	S band	Large vessel	41.02	3.03	7.4%	2.6
7A	5 × 5	Legacy	X band	Small vessel	28.78	1.44	5.0%	0.9
8A	5 × 5	Legacy	X band	Large vessel	38.38	2.15	5.6%	1.8
5B	10 × 10	Legacy	S band	Small vessel	29.33	3.04	10.4%	4.2
6B	10 × 10	Legacy	S band	Large vessel	41.02	6.18	15.1%	10.3
7B	10 × 10	Legacy	X band	Small vessel	28.78	2.49	8.7%	2.9
8B	10 × 10	Legacy	X band	Large vessel	38.38	4.02	10.5%	7.0
13A	5 × 5	Modern	S band	Small vessel	29.33	1.71	5.8%	2.3
14A	5 × 5	Modern	S band	Large vessel	41.02	3.90	9.5%	4.9
15A	5 × 5	Modern	X band	Small vessel	28.78	1.31	4.6%	1.7
16A	5 × 5	Modern	X band	Large vessel	38.38	2.82	7.3%	3.4
13B	10 × 10	Modern	S band	Small vessel	29.33	3.04	10.4%	7.5
14B	10 × 10	Modern	S band	Large vessel	41.02	7.06	17.2%	19.0
15B	10 × 10	Modern	X band	Small vessel	28.78	2.43	8.4%	5.2
16B	10 × 10	Modern	X band	Large vessel	38.38	4.94	12.9%	13.0

even if no such steps are undertaken, the farms are usually designed to maintain a 2 NM buffer between the turbines and the designated shipping routes. Observance of those conditions will address most of the false echo scenarios relevant to vessel-borne radars and will strongly minimize their negative impact.

- A practical observation can also be made that an offshore wind farm, i.e. an object of significant physical dimensions, is clearly visible on radar displays even from the distance of several kilometers. Consequently, radar operators are usually trained to routinely identify them and to properly interpret the visualizations produced by radar equipment.

5.3. Radio Shadowing Simulation Results

Figures 15–18 show simulation results for selected scenarios (see Tab. 2). They provide a graphic visualization of useful radar coverage as well as its reduction caused by the presence of an offshore wind farm. This range limitation can be described by means of depth, shape and angular width.

Figure 15 shows the ranges of coastal radar for various types of objects. It can be seen that in the case of a small vessel being the target, the radar ranges merely reach the wind farm area for both X and S band radars. When the tracked object is a large vessel, the range of the both X and S band radars extends well beyond the wind farm. Figure 16 illustrates the ranges of coastal S band radar for various types of wind turbines and for different scenarios regarding the number of turbines and their spatial arrangement. In all of the analysed cases, the respective S band radar ranges are comparable, the only difference is the nature of signal propagation in the area behind the wind farm.

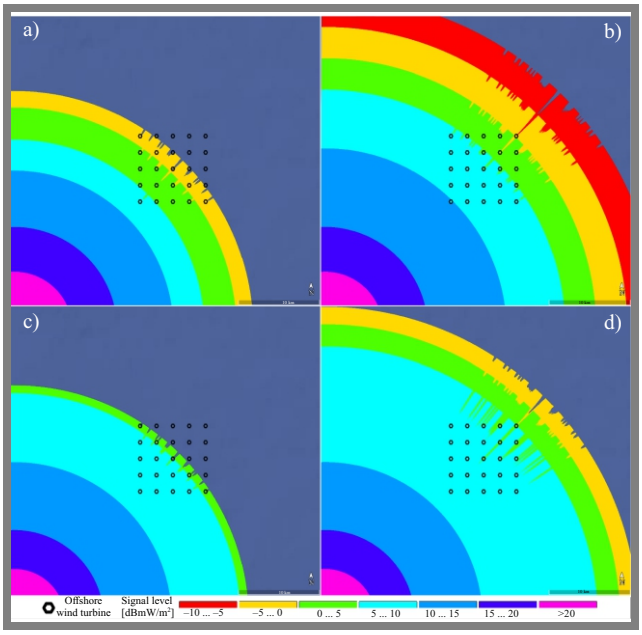

Fig. 15. Comparison of S and X band radar ranges and different types of objects (RCS): a) scenario 13A, b) scenario 14A, c) scenario 15A, and d) scenario 16A.

Table 6 shows coastal radar's nominal ranges and their maximal reduction (along a diagonal line of the farm area) caused by the presence of wind turbines. As one may notice, some similarities may be observed between the presented results. First of all, an increase of the number of wind turbines from

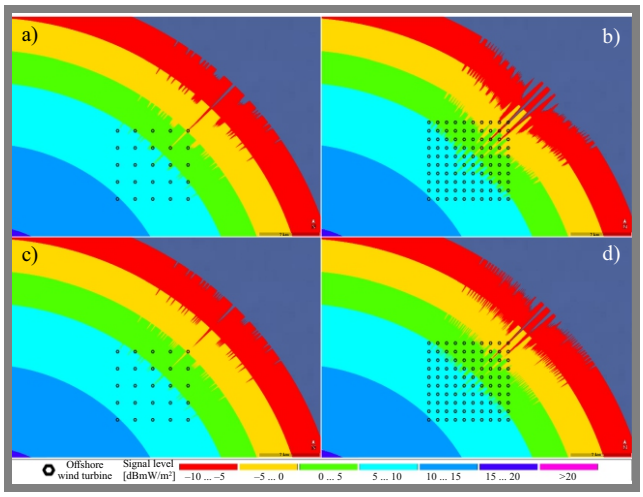

Fig. 16. Comparison of S radar ranges for a large object (RCS), various 5 × 5 and 10 × 10 turbine systems and types: modern scenario a) 14A, b) 14B, and legacy scenario c) 6A, d) 6B.

25 (5 × 5 turbines scenarios) to 100 (10 × 10 scenarios) causes the elongation of the maximum radar range reduction, along the diagonal line of the farm area, of approx. 80% for all of the cases, i.e. legacy/modern turbines and small/large vessel detection using S band/X band radar. A larger number of wind turbines also results in greater distortions which are visible especially on the edge of the radar's coverage range – see Fig. 16, compare a) vs. b) and c) vs. d). This translates into an over threefold increase in the radar coverage area affected (reduced) by the presence of a wind farm in small vessel detection scenarios and an almost fourfold increase in the case of large vessels. On the other hand, the difference between the presence of modern turbines is almost negligible (compared to legacy ones) for the small vessel detection scenarios (i.e. 5 × 5/10 × 10 turbines and S band/X band radar). The said difference is, however, slightly noticeable for the large vessel detection scenarios (5 × 5/10 × 10 turbines and S band/X band radar) – the radar reduction range is increased by approx. 20%. The main difference between these two types of turbines lies in the angular width of the resulting radio shadow regions. For the proposed turbine arrangements and a coastal radar located 12 NM from the boundary of the offshore wind farm, the main radio shadow lobe is created along the diagonal of the farm area. In the case of legacy turbines (122 m rotor diameter) the angular width of largest radio shadow area covers less than 0.5° and in the case of modern turbines (236 m rotor diameter) it covers slightly more than 0.7°.

In all vessel-borne radar scenarios (1–4, 9–12) the influence of the offshore wind farm is similar and the only difference stems from radar coverage which depends on the operating band (S band/X band) and the size of the object detected. For the proposed turbine arrangements and vessel-borne radars located in close proximity, i.e. 2 NM from the boundary of the offshore wind farm, turbine masts – usually made of concrete and steel – play a key role in creating radio shadow areas.

Figure 17 shows examples of ranges of on-board radar in a scenario in which a large vessel is being detected and for various turbine arrangements: 5 × 5 and 10 × 10. The presence

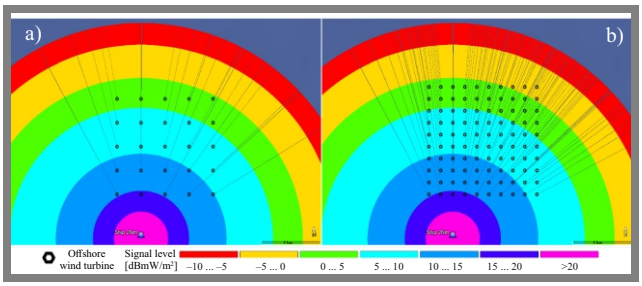

Fig. 17. Comparison of vessel-borne S radar ranges while detecting a large vessel (RCS), various 5 × 5 and 10 × 10 turbine systems: a) scenario 10A and b) scenario 10B.

of very narrow, stripe-like areas with no radio coverage can be clearly noticed. It is caused by wind turbine masts obstructing the line-of-sight between the radar and the target. The number of these areas depends on the quantity of the turbines: the more turbines, the more areas without radar coverage. There is almost no difference between the two types of turbines analyzed, because their masts have similar dimensions – the maximum tower radius of a legacy turbine is about 3.1 m and it equals 3.25 m for a modern turbine. It is worth noting that in all "vessel cases", the reduction of the radar range is already observed, starting from the turbine closest to the radar.

Table 7 shows vessel-borne radar nominal ranges and the coverage affected by the presence of a wind farm. As one may see, an increase in the number of wind turbines from 25 (5 × 5 scenarios) to 100 (10 × 10 scenarios) results in a nearly fourfold increase in the radar area affected (reduced) by the presence of a wind farm – for both operating bands and both sizes of detected objects.

If the simulations demonstrate a negative impact of an OWF on a radiolocation system, adequate corrective (mitigation) measures should be implemented. In most cases, such measures entail an installation of an additional radar at the edge of the wind farm. In order to achieve the desired mitigation effect, it is necessary to specify the exact technical parameters of the additional "corrective" radar, which should include (at least) the following:

- coordinates (location) of the proposed corrective radar,
- height of the radar antenna,
- azimuth of the radar antenna (not applicable to omnidirectional antennas),
- transmitter power and antenna gain,
- 3–dB width of the antenna beam in the horizontal plane (not applicable for omnidirectional antennas).

It should be added that in the context of corrective measures, two aspects are of particular importance:

- any recommendations regarding the potential corrective measures should be supported and verified by simulation analysis,
- the recommended corrective measures should be designed in such a way that the "new" radar will not generate additional negative effects that may potentially degrade the system.

Tab. 7. Results for vessel-borne radar simulations.

Scenario number	Turbine configuration	Turbine type	Radar type	Target type	Nominal radar range [km]	Affected radar area [km^2]
1A	5 × 5	Legacy	S band	Small vessel	9.84	0.4
2A	5 × 5	Legacy	S band	Large vessel	18.11	2.7
3A	5 × 5	Legacy	X band	Small vessel	12.32	0.9
4A	5 × 5	Legacy	X band	Large vessel	20.15	3.5
1B	10 × 10	Legacy	S band	Small vessel	9.84	1.4
2B	10 × 10	Legacy	S band	Large vessel	18.11	10.2
3B	10 × 10	Legacy	X band	Small vessel	12.32	3.2
4B	10 × 10	Legacy	X band	Large vessel	20.15	13.3
9A	5 × 5	Modern	S band	Small vessel	9.84	0.4
10A	5 × 5	Modern	S band	Large vessel	18.11	2.7
11A	5 × 5	Modern	X band	Small vessel	12.32	0.9
12A	5 × 5	Modern	X band	Large vessel	20.15	3.5
9B	10 × 10	Modern	S band	Small vessel	9.84	1.4
10B	10 × 10	Modern	S band	Large vessel	18.11	10.2
11B	10 × 10	Modern	X band	Small vessel	12.32	3.2
12B	10 × 10	Modern	X band	Large vessel	20.15	13.3

Figure 18 shows an example of a corrective measure eliminating radio shadowing effects existing north-east of the OWF. In this case, the additional radar[3] was installed at the wind farm's edge and its angular range was set in the way shown in the image (from 315° to 135°, to avoid additional interference when the radar is operating). As one may see, the radar helps fully eliminate radio shadowing behind the OWF, proving that the mitigation measure was successful.

6. Conclusions

In accordance with the performed simulations, an increase in the number of the wind turbines (from 25 to 100) may elongate the zone in which the radar's range is reduced, along the diagonal of the farm area, by approx. 80% for all "coastal radar cases", i.e. for legacy/modern turbines and small/large vessel detection scenarios, using S band/X band radar. Consequently, it translates into an over threefold increase in radar coverage affected (reduced) by the presence of a wind farm in small vessel detection scenarios and an almost fourfold increase in the case of large vessel detection scenarios.

As it was predicted, an increase in the wind turbines' dimensions and the growing number of offshore wind farms may affect a wide range of radiocommunication and radar systems operating in maritime environments. That being said, there is a need to point out a few important aspects. OWFs are essentially becoming an additional "navigational landmark".

[3]Radar parameters adopted for the simulation are the same as those required by OWF operators in Poland: X band, power 70 dBm, gain 29 dBi, antenna height 15 m.

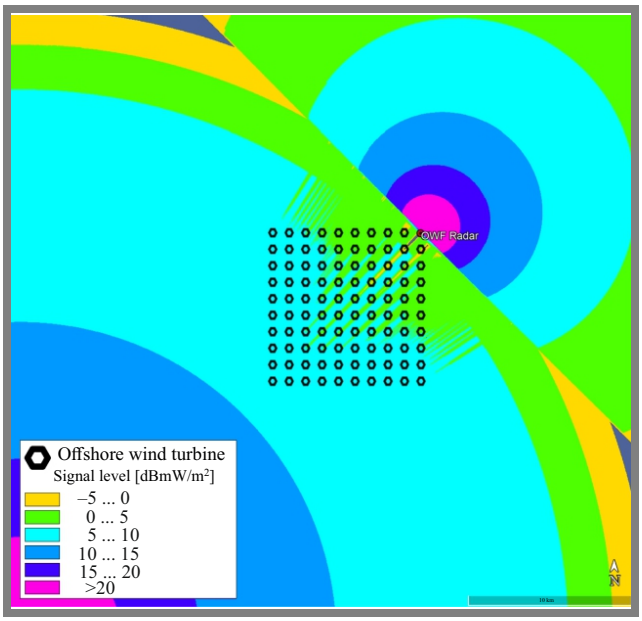

Fig. 18. Visualization of a corrective measure – radar X.

Suitable paint schemes, lighting and AtoN signals complying with IALA guideline G1162 – the marking of offshore man-made structures [23] – will force seafarers to operate with higher caution levels. Wind turbines are also clearly visible on radar from many kilometers away and investors are obligated to implement monitoring systems within the farms themselves, which is also beneficial for the overall safety in these areas.

In some scenarios, where the above guidance is not sufficient, it is necessary to implement corrective measures. With re-

spect to the topic of this article, such measures are mostly required to mitigate radio shadowing effects that may significantly shorten the operational range of coastal radars. In cases requiring correction, an additional radar (sometimes more than one) with suitable technical parameters, should be installed. The location of the corrective radar should be carefully selected. Usually, it would be positioned at the farm's edge, or inside its boundaries to maximize the mitigation effect and to make sure that the costs are acceptable. The corrective radar should not generate additional negative effects potentially degrading the system. This is also a very important requirement while designing specific compensation measures.

Usually, no corrective measures are recommended for vessel-borne (on-board) radars. Installation of an additional radar would not be rational in that case, as the vessel may be located, in any given moment, anywhere relative to the OWF. Also, since the vessel itself is in motion, in the majority of cases it is only affected by an OWF over a short period of time. The following should be taken into consideration as far as vessel-borne radar systems are concerned:

- Vessel-borne radars will be impacted by radio shadowing only in areas opposite to the wind farm. As a result, a ship may be unaware of only those objects that are located behind the farm, which is not a serious threat for the safety of navigation.
- An OWF, as a physical object of substantial dimensions, will be easily detected by on-board radar systems.

In the case of false radar echoes, corrective measure are usually not recommended either, even though the ranges of the echoes may be significant, particularly for coastal radars. The reasons for that approach were explained in Section 5. Below, a summary of the most important points is presented:

- False echo simulations (for the coastal radar case) were conducted for the worst-case scenario, where the angle between the rotor plane and the turbine-radar section amounts to 90°. Under such an assumption, the reflection from the turbine is maximized, as is the radar cross section (RCS) of the turbine. In fact, in this case, RCS is several magnitudes of order greater than the actual area of the turbine's rotor. Consequently, the ranges of the false echoes presented in the article are absolute theoretical maximums of this phenomenon. The probability that the exact conditions required for the maximum reflection will be satisfied in realistic scenarios is rather low. So, in the majority of cases, the actual impact of the false echoes will be much lower and sometimes even negligible.
- Even though the theoretical false echo ranges for coastal radars (Annex 1) can be very long, their angular width is actually very low (2–4°), so their actual impact on the operation of radars is mostly negligible.
- OWFs are clearly visible on radar displays, even from the distance of several kilometers. Consequently, radar operators are usually trained to routinely identify them and to properly interpret the visualizations produced by radar.
- False echoes are generally a very dynamic phenomenon and depend on the location of the object (e.g. a vessel) with respect to the wind turbine and/or radar. Obviously, this location varies. Therefore, conventional corrective measures involving an additional radar would be pointless here.

Besides corrective measures, verification measurements are another element intended to ensure smooth coexistence of OWFs and maritime radiolocation systems. They are required under Polish law and have to be conducted after a given OWF has been erected, but before it starts generating power. The goal of these measurements is to assess the actual impact of the farm on relevant systems. If it turns out that its impact is more damaging than the associated expert opinion indicated, additional compensation measures will be necessary. The institution for which the authors of this paper work is going to be involved in such verification measurements on Polish waters.

It should be emphasized that the analysis of the impact that offshore wind farms exert on radiocommunication systems is a very complex and multidimensional issue. In addition to their influence on maritime radar installations, the impact on systems operating in the VHF and UHF bands [4], as well as communication based on MF/HF frequencies, should be considered. In future work, the authors will analyze the impact that the presence of OWFs exerts on MF/HF systems which are another important component improving safety at sea.

Acknowledgments

This article is part of a statutory work (number 08300013) that has been partially funded by the Polish Ministry of Education and Science.

References

[1] Global Wind Energy Council, *Global Wind Report 2023*, (https://gwec.net/globalwindreport2023/).

[2] Recommendation ITU-R BT.1893-1, *Assessment Methods of Impairment Caused to Digital Television Reception by Wind Turbines*, 2015 (https://www.itu.int/rec/R-REC-BT.1893/en).

[3] K. Bronk, A. Lipka, R. Niski, and B. Wereszko, "Wind Farms Influence on Radiocommunication Systems Operating in the VHF and UHF Bands", *Journal of Telecommunication and Information Technology*, no. 2, pp. 30–43, 2015 (https://jtit.pl/jtit/article/view/787/780).

[4] K. Bronk, P. Koncicki, A. Lipka, R. Niski, and B. Wereszko, "Radio Channel Modelling for VHF System Operating in the Offshore Wind Farms Propagation Environment", *Sensors*, vol. 23, no. 17, art. no. 7593, 2023 (https://doi.org/10.3390/s23177593).

[5] J. Szóstka, "Electromagnetic Compatibility of Wind Farms" *Przegląd Telekomunikacyjny i Wiadomości Telekomunikacyjne*, no. 6, pp. 235–240, 2011 [in Polish].

[6] M. J. Howard, G. J. Poupart, and C.R. Brewitt-Taylor, *Investigation of the Impact of Wind Turbines on the MSSR Installations at Dooncarton*, Mt Gabriel and Woodcock Hill, QinetiQ Ireland, Final Report. September 2004.

[7] W. He, C. Ji, Z. Huo, X. Wang, and R. Wu, "RCS Calculation of Wind Turbine Mast for Weather Radar", in: *2016 CIE International*

Conference on Radar (RADAR), Guangzhou, China, 2016 (https://doi.org/10.1109/RADAR.2016.8059374).

[8] G. Greving, W.-D. Biermann, and R. Mundt, "Radar and Wind Turbines – RCS Theory and Results for Objects on the Ground and in Finite Distance", in: *Microwaves, Radar and Remote Sensing Symposium*, Kiev, Ukraine, 2011 (https://doi.org/10.1109/MRRS.2011.6053665).

[9] R.A. Ross, "Forward Scattering at Grazing Incidence on Flat Plates", *IEEE Transactions on Antennas and Propagation*, vol. 56, no. 2, pp. 606–609, 2008 (https://doi.org/10.1109/TAP.2007.915479).

[10] D.M. Pozar, *Microwave Engineering*, 4th ed., Hoboken: Wiley, 752 p., 2012 (ISBN: 9780470631553).

[11] Vestas, *General Description V236-15 MW*, Document no.: 0104-1036v02 2021-06-04 (https://www.vestas.com/en/products/offshore/V236-15MW).

[12] Specialchem, *Omnexus – the material selection platform*, [online] Available: (https://omnexus.specialchem.com/polymer-properties/properties/dielectric-constant/ (accessed on 02.08.2023).

[13] T. Eltsov and T.W. Patzek, "Beyond Steel Casing: Detecting Zonal Isolation in the Borehole Environment", in: *SPE Middle East Oil and Gas Show and Conference*, Manama, Bahrain, 2019 (https://doi.org/10.2118/195036-MS).

[14] A. Sarolic, "Wind Turbine Radar Cross Section for Air Traffic Control Secondary Surveillance Radar", in: *2019 European Microwave Conference in Central Europe (EuMCE)*, Prague, Czech Republic, 2019 (https://ieeexplore.ieee.org/abstract/document/8874790).

[15] D. Trappeniers, E. Van Lil, and A. van de Cappelle, "Effects of Objects with Moving Parts Like Wind Turbines on Maritime RF Safety and Navigation Systems", *Proceedings of The European Conference on Antennas and Propagation: EuCAP*, Nice, France, 2006.

[16] "Radartutorial", https://www.radartutorial.eu (accessed on 02.08.2023).

[17] Recommendation ITU-R P.2001-4, *A General Purpose Wide-range Terrestrial Propagation Model in the Frequency Range 30 MHz to 50 GHz*, ITU, 2021 (https://www.itu.int/rec/R-REC-P.2001/en).

[18] H. Dorner, "Efficiency and Economic Comparison of Different WEC (Wind Energy Converters) Rotor Systems", in: *International Conference on Appropriate Technologies for Semiarid Areas, Conference Report*, Berlin, 1975 (http://www.heiner-doerner-windenergie.de/comparisonHAWTVAWT.pdf

[19] W. Adamczak, "Possibilities and Effectiveness of Direct Conversion of Aerogenerator Rotor Motion into Electricity", M.Sc. Thesis, 2004, Poznan University of Technology [in Polish].

[20] I. Harre, "RCS in Radar Range Calculations for Maritime Targets (V2.0-20040206)", Bremen, 2004 (http://www.mar-it.de/Radar/RCS/RCS_xx.pdf).

[21] P.D.L. Williams, H.D. Cramp, and K. Curtis, "Experimental Study of the Radar Cross Section of Maritime Targets", *IEE Journal on Electronic Circuits and Systems*, vol. 2, no. 4, pp. 121–136, 1978 (https://doi.org/10.1049/ij-ecs.1978.0026).

[22] R.J. Katulski, *Propagation of Radio Waves in Wireless Telecommunications*, Sulejówek: WKŁ, 232 p., 2014 (ISBN: 9788320619348) [in Polish].

[23] IALA, *Guideline G1162 – The Marking of Offshore Man-made Structures*, 2021 (https://www.iala-aism.org/product/g1162/)

Krzysztof Bronk, Ph.D., Assistant Professor
Wireless Systems and Networks Department
https://orcid.org/0000-0002-3594-8462
E-mail: K.Bronk@il-pib.pl
National Institute of Telecommunications, Warsaw, Poland
https://www.gov.pl/web/instytut-lacznosci

Patryk Koncicki, M.Sc., Senior Specialist
Wireless Systems and Networks Department
https://orcid.org/0000-0003-2618-1594
E-mail: P.Koncicki@il-pib.pl
National Institute of Telecommunications, Warsaw, Poland
https://www.gov.pl/web/instytut-lacznosci

Adam Lipka, Ph.D., Assistant Professor
Wireless Systems and Networks Department
https://orcid.org/0000-0002-2919-4270
E-mail: A.Lipka@il pib.pl
National Institute of Telecommunications, Warsaw, Poland
https://www.gov.pl/web/instytut-lacznosci

Rafał Niski, Ph.D., Assistant Professor
Wireless Systems and Networks Department
https://orcid.org/0000-0002-5106-9046
E-mail: R.Niski@il pib.pl
National Institute of Telecommunications, Warsaw, Poland
https://www.gov.pl/web/instytut-lacznosci

Błażej Wereszko, M.Sc., Leading Specialist
Wireless Systems and Networks Department
https://orcid.org/0000-0001-7474-692X
E-mail: B.Wereszko@il-pib.pl
National Institute of Telecommunications, Warsaw, Poland
https://www.gov.pl/web/instytut-lacznosci